Transmission spectra of bistable systems: From the ultraquantum to the classical regime

Evgeny V. Anikin,[1] Natalya S. Maslova,[2] Nikolay A. Gippius,[1] and Igor M. Sokolov[3]
[1]*Skolkovo Institute of Science and Technology, 121205 Moscow, Russia*
[2]*Quantum Technology Centrum and Chair of Quantum Electronics, Department of Physics, Lomonosov Moscow State University, 119991 Moscow, Russia*
[3]*Institut für Physik and IRIS Adlershof, Humboldt Universität zu Berlin, Newtonstraße 15, 12489 Berlin, Germany*

(Received 30 April 2020; accepted 31 August 2020; published 28 September 2020)

We present an analytical and numerical study of the fluorescence spectra of a bistable driven system by means of the Keldysh diagram technique in pseudoparticle representation. The spectra exhibit smooth transition between the ultraquantum and the quasiclassical limits and indicate the threshold value of the external field when changing of the most probable stable state occurs. The analysis of the fluorescence spectra also allows us to determine the most probable stable state of the system. It was also shown that, at integer and half-integer detuning-nonlinearity ratios, multiphoton resonance leads to abrupt changes in fluorescence spectra. It was also revealed that the fluorescence spectra are symmetric in the limit of zero environment temperature. The predicted features of the spectra could be observed in experiments with ultrahigh-quality resonators in either microwave or optical domains.

DOI: 10.1103/PhysRevA.102.033725

I. INTRODUCTION

Classical and quantum systems with two or more stable states have been under intense investigation for several decades. Bistability and multistability often appear in the presence of an external coherent driving field [1,2]. Discovered first in Fabry-Perot cavities filled with nonlinear medium [3], the phenomenon of bistability has been observed in a wide range of experimental setups including laser cavities [4], whispering gallery resonators [5], exciton-polaritons in semiconductor microcavities [6], etc. Recently, bistability at small photon numbers ($\sim 10^2$) has been observed in mesoscopic Josephson junction array resonators [7] with ultrahigh-quality factors ($\sim 10^4$). Quantum optical and electronic systems exhibiting bistability are promising candidates for developing logic elements, switching and memory devices, various turnstiles, etc. A driven oscillator mode with Kerr-like nonlinearity is one of the simplest models describing bistability in various physical systems. The key features of bistable systems including S-shaped response curves and hysteresis cycles under varying external field amplitudes can be analyzed by means of this model. This model also allows one to obtain the stationary occupations and switching rates between two stable states due to interaction with dissipative environment [8–11].

The stationary populations of different stable states and switching rates in the model of a driven nonlinear oscillator in the presence of external noise have been thoroughly studied. The stationary density matrix at zero environment temperature is obtained from the quantum kinetic equation of the Fokker-Planck type for the generalized Glauber P function [12]. For small damping, numerical analysis based on the rate equation was performed in Ref. [8]. The method suggested in Ref. [8] allows one to calculate the switching rates and the stationary occupations of the stable states for arbitrary temperature, which extends the analysis of Ref. [12]. The quasiclassical limit of the model was considered in Ref. [9], where it was demonstrated that in the limit of large photon numbers and high temperature the model reduces to a classical stochastic one. Such an approximation allows one to find analytical expressions for the stationary occupations of the quasienergy states and transition rates between two stable states for low damping.

Despite the well-studied statistical properties of the considered bistable system, there is a lack of detailed analysis of its fluorescence and transmitted light spectra. In Ref. [12], the spectrum was obtained by linearization of the Fokker-Planck-type kinetic equation for the generalized Glauber function. A similar approach was exploited in Ref. [1], where a mean-field model of atoms in a resonant cavity was discussed. In Ref. [13], a factorization procedure of an infinite set of the equations for correlation functions is used to get the spectrum. However, such procedures are valid only in the limit of large damping constants and small quantum fluctuations. In the opposite limit of small damping, one should expect that the fluorescence spectrum is a combination of multiple narrow Lorenzian peaks corresponding to transitions between the quasienergy states, which totally differs from the quasi-Lorenzian linearized spectrum of Ref. [12].

The spectrum in this limit is not studied enough nowadays nor has it been studied enough in the intermediate regime where linearization cannot be performed and the quasienergy states are not well defined. However, this regime is of particular interest in the context of bistability in Josephson junction array resonators [7] because the nonlinearity per quantum in these resonators is comparable to the linewidth [14]. It

is possible to find the spectrum in this regime by solving numerically the master equation introduced in Ref. [12]. The details of spectrum behavior near the external field threshold value corresponding to the switching between the stable states have not been clearly understood up to now. Moreover, the influence of multiphoton resonance leading to degeneracy of quasienergy states [15] on fluorescence spectra also needs careful investigation.

In the present manuscript, we demonstrate that fluorescence spectra of a bistable driven system indicate the external field threshold value and allow one to find the most probable state of the system. Our analysis is based on the calculation of the polarization operator $\Pi^<$ by means of the Keldysh diagram technique in pseudoparticle representation. The Keldysh diagram technique allows self-consistent treatment of the energy spectrum modification due to interaction processes and the nonstationary changing of occupation numbers. Also, it allows one to treat in a regular way the corrections arising from finite bath correlation time. In the Keldysh diagram technique approach, such corrections are represented by subseries of maximally crossing diagrams similar to cooperons in the theory of weak localization and are proportional to correlation time in the leading order. In the general case, the equations for the fluorescence spectrum are solved numerically, but analytical expressions are also presented in two limiting cases of small and large ratios between the detuning and damping constants. This allows one to track the smooth transition between the classical and the quantum fluorescence spectra behavior and to analyze the spectrum properties for nearly degenerate quasienergy states.

II. THE THEORETICAL MODEL

We consider a simple model of a bistable driven system consisting of a resonant mode with Kerr-like nonlinearity [8,12]. The effective Hamiltonian of such a system in the rotating-frame approximation reads

$$\hat{H}_0 = -\Delta \hat{a}^\dagger \hat{a} + \frac{\alpha}{2}(\hat{a}^\dagger \hat{a})^2 + f(\hat{a} + \hat{a}^\dagger). \tag{1}$$

Here Δ is the detuning between the driving field and the resonant oscillator frequency, α is the Kerr coefficient, and f is proportional to the amplitude of the driving field.

In the classical limit, one should replace the operators $\hat{a}$ and $\hat{a}^\dagger$ in Eq. (1) with the classical field amplitudes a and a^* to obtain the classical Hamiltonian. The S-shaped response curve is depicted in Fig. 1. In the inset, the classical phase portrait of the system is shown: The classical trajectories in the a plane are given by the contour lines of the classical Hamiltonian. In the phase portrait, there are two stable stationary states, states 1 and 2, and one unstable stationary state, state S. The only dimensionless parameter of the classical Hamiltonian, $\alpha f^2/\Delta^3 \equiv \beta$, governs the system dynamics. The bistability range is limited by the maximal value of $\beta = \beta_{\rm crit} \equiv 4/27$. For the quantum Hamiltonian, there exists another dimensionless parameter, $m \equiv 2\Delta/\alpha$. The quasiclassical limit is acquired at large noninteger values of m.

Let us assume that the system is weakly interacting with the environment, so the full Hamiltonian reads

$$\hat{H}_{\rm full} = \hat{H}_0 + \hat{\xi}^\dagger \hat{a} + \hat{\xi} \hat{a}^\dagger. \tag{2}$$

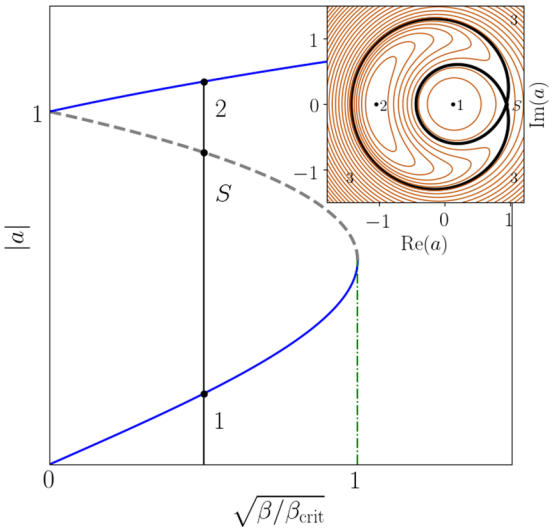

FIG. 1. The S-shaped response curve to the external driving field of the nonlinear oscillator model (1) is shown. The oscillator field amplitude a is given in units of $\sqrt{\Delta/\alpha}$. Blue solid lines denote the stable states 1 and 2, and the gray dashed line corresponds to the unstable state S. The classical phase portrait of the system is shown in the inset for $\sqrt{\beta/\beta_{\rm crit}} = 0.3$, where the stationary states are denoted by black dots.

For the case of white noise, the damping operators $\hat{\xi}$ and $\hat{\xi}^\dagger$ are δ-correlated:

$$\langle \hat{\xi}(t)\hat{\xi}^\dagger(t')\rangle = \gamma(N+1)\delta(t-t'),$$
$$\langle \hat{\xi}^\dagger(t)\hat{\xi}(t')\rangle = \gamma N \delta(t-t'). \tag{3}$$

Here N is the number of thermal photons at the external field frequency.

With such assumptions, the evolution of the system density matrix can be described by the master equation [8,12,16–18]:

$$\partial_t \hat{\rho} = \mathcal{L}\hat{\rho} = -i[\hat{H}_0, \hat{\rho}] + \frac{\gamma}{2}(2\hat{a}\hat{\rho}\hat{a}^\dagger - \hat{\rho}\hat{a}^\dagger\hat{a} - \hat{a}^\dagger\hat{a}\hat{\rho} + 2N[[\hat{a}, \hat{\rho}], \hat{a}^\dagger]). \tag{4}$$

This equation can be derived in the quasienergy representation. It follows from the kinetic equation for the lesser Green's function $G^<_{nn'}(t,t)$ obtained by means of the Keldysh diagram technique generalized for the pseudoparticle approach with an additional constraint on the physically available states (see Appendix A), where $|n\rangle$ are the eigenstates of the system Hamiltonian $\hat{H}_0$.

The incoherent part of the photoluminescence spectrum is given by the correlation function of the operators $\hat{a}$ and $\hat{a}^\dagger$ [12]:

$$S(\omega) = \int dt e^{i\omega t} \langle \hat{a}^\dagger(0)\hat{a}(t)\rangle. \tag{5}$$

To obtain $S(\omega)$, one must calculate the polarization operator $\Pi^<(\omega)$ in the pseudoparticle Keldysh diagram technique (see Appendix B), which coincides with $S(\omega)$ in the stationary case.

The detailed calculation of $\Pi^<$ given in Appendix B leads to the following expression for the fluorescence spectrum:

$$S(\omega) = 2\,\mathrm{Re}\,\mathrm{Tr}\,\{\hat{a}[-i\omega\check{\mathbb{1}} - \check{\mathcal{L}}]^{-1}\hat{\rho}_{\mathrm{st}}\hat{a}^\dagger\}. \tag{6}$$

Here the superoperator $\mathcal{L}$ is determined by Eq. (B8) and has the following explicit form for white noise:

$$\begin{aligned}\mathcal{L}_{ij,kl} = &-i(\epsilon_i - \epsilon_j)\delta_{ik}\delta_{lj} \\ &+ \frac{\gamma(N+1)}{2}[2a_{ik}a^*_{jl} - (\hat{a}^\dagger\hat{a})_{ik}\delta_{lj} - \delta_{ik}(\hat{a}^\dagger\hat{a})_{lj}] \\ &+ \frac{\gamma N}{2}[2a^*_{ki}a_{lj} - (\hat{a}\hat{a}^\dagger)_{ik}\delta_{lj} - \delta_{ik}(\hat{a}\hat{a}^\dagger)_{lj}].\end{aligned} \tag{7}$$

The stationary density matrix can be obtained from the kinetic equation (4). The incoherent part of the spectra can be calculated numerically by means of Eq. (6).

There exist two complementary approximations allowing one to get analytical expressions for $S(\omega)$. They correspond to the quantum limit of well-defined quasienergy states and the quasiclassical limit of small quantum and thermal fluctuations considered in Ref. [12].

The first approximation is valid providing that γ is smaller than any of the differences between eigenvalues of the effective Hamiltonian, and the spectrum consists of distinct Lorenzian peaks corresponding to transitions between quasienergy levels. When ω is close to a transition frequency between the levels $|n\rangle$ and $|n'\rangle$, the following expression for the spectrum is valid (see Appendix B):

$$S(\omega) = \sum_{n'n} P_{n'}|a_{nn'}|^2 \frac{2\Gamma_{n'n}}{(\omega - \epsilon_n + \epsilon_{n'})^2 + \Gamma^2_{n'n}}, \tag{8}$$

where the widths of the Lorenzian peaks are defined as

$$\begin{aligned}2\Gamma_{n'n} = &\gamma(N+1)[(\hat{a}^\dagger\hat{a})_{n'n'} + (\hat{a}^\dagger\hat{a})_{nn} - 2\,\mathrm{Re}\,a_{n'n'}a^*_{nn}] \\ &+ \gamma N[(\hat{a}\hat{a}^\dagger)_{n'n'} + (\hat{a}\hat{a}^\dagger)_{nn} - 2\,\mathrm{Re}\,a^*_{n'n'}a_{nn}],\end{aligned} \tag{9}$$

and $P_{n'}$ are the stationary occupation probabilities of the unperturbed Hamiltonian eigenstates $|n'\rangle$. The occupation probabilities in this approximation are defined by the stationary rate equation (see Ref. [8]) which is the diagonal approximation of the quantum master equation (4). The Keldysh diagram technique is the most clear and straightforward way to obtain strong linewidth narrowing for the transitions between two well-defined quasienergy states from classical region 2 [Eqs. (9) and (B11)]. This effect can be seen from Fig. 2 where the linewidths of the transitions between different quasienergy states are shown. The narrowing of the linewidth is described by $\Delta\gamma_{nn'}$ [Eq. (B11)] and appears by summing the series of ladder diagrams in the polarization operator $\Pi^<$ (see Appendix B). The total linewidth is not the sum of the widths γ_n and $\gamma_{n'}$ of the quasienergy states involved in the transition. For the states within region 2, the term $\Delta\gamma_{nn'}$ leads to strong narrowing of the fluorescence spectrum peaks, because for these states the diagonal matrix element of $\hat{a}$ strongly deviates from zero. On the other hand, for the states within region 1 these matrix elements are close to zero for small external field amplitudes, so the narrowing is not well pronounced. In addition, for transitions between quasienergy states from different regions of the phase space, $\Delta\gamma_{nn'}$ changes sign, which leads to slightly increased linewidths.

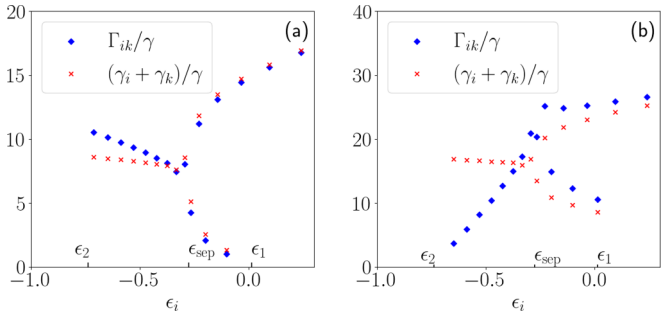

FIG. 2. Linewidths of the fluorescence spectrum peaks of the quantum driven nonlinear oscillator corresponding to transition between the quasienergy state n and the other quasienergy states are shown (blue diamonds), where n corresponds to classical stable states 1 (a) and 2 (b). The model parameters are as follows: $2\Delta/\alpha = 15.4$ and $f/f_{\mathrm{crit}} = 0.3$. Sums of linewidths of individual quasienergy levels are shown for comparison (red crosses). The values of the quasienergies on the horizontal axis are given in units of Δ^2/α.

Another approximation exploited in Ref. [12] is based on the quantum Fokker-Planck equation for the density matrix in the generalized P representation:

$$\begin{aligned}\frac{\partial P(a,a^*)}{\partial t} = &\Big[i\frac{\partial}{\partial a}[(-\Delta - i\gamma/2)a + \alpha a^2 a^* + f] \\ &- \frac{i\alpha}{2}\frac{\partial^2}{\partial a^2}a^2 + \frac{\gamma N}{2}\frac{\partial^2}{\partial a\partial a^*}\Big]P(a,a^*) + \mathrm{c.c.}\end{aligned} \tag{10}$$

This equation can be linearized near each of the classical stable states which can be obtained from the solution of stationary classical equations of motion:

$$-(\Delta + i\gamma/2)a + \alpha a^2 a^* + f = 0. \tag{11}$$

The resulting expression for the spectrum reads

$$\begin{aligned}S(\omega) = \sum_{q=1,2}\frac{1}{4\pi^2|\lambda_q(\omega)|^2}\gamma\big[&(1+N)\alpha^2 n_q^2 \\ &+ N|\omega - \Delta + 2\alpha n_q - i\gamma/2|^2\big]P_q,\end{aligned} \tag{12}$$

with

$$\begin{aligned}\lambda_q(\omega) = &-(\omega - \Delta + 2\alpha n_q - i\gamma/2)(\omega + \Delta - 2\alpha n_q - i\gamma/2) \\ &- \alpha^2 n_q^2,\end{aligned} \tag{13}$$

where $q = 1$ and 2 correspond to two stationary states, P_q are classical probabilities to find the system near each of the stable states q, and n_q is the mean value of $\hat{a}^\dagger\hat{a}$ in the stable state q.

III. RESULTS AND DISCUSSION

Using the approach described in the previous section, we calculated the incoherent part of the emission spectrum of the quantum driven nonlinear oscillator. We considered different values of the model parameters including the small-fluctuation regime and the weak-coupling regime.

First of all, we explored the transition between the small-fluctuation and weak-coupling regimes which occurs at the decreasing dimensionless damping constant $\vartheta \equiv \gamma/\Delta$ (see Fig. 3). At small ϑ, the exact spectrum matches with the

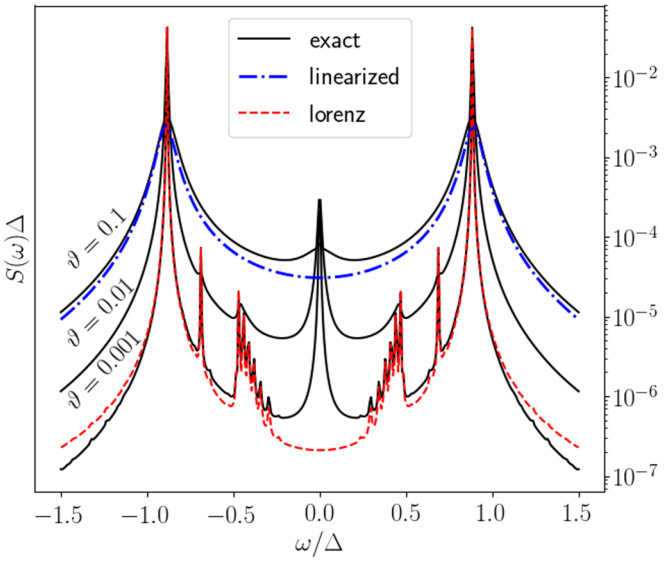

FIG. 3. The fluorescence spectra of the quantum driven nonlinear oscillator model are shown for $m = 12.5$, $N = 0$, $f/f_{\text{crit}} = 0.2$, and different values of ϑ. Black solid lines denote the spectra obtained from Eq. (6), the red dashed line represents the spectrum obtained from the Lorenzian approximation, and the blue dash-dotted line represents the spectrum obtained from the linear approximation. At small ϑ, the spectrum consists of multiple narrow Lorenzian peaks corresponding to transitions between different quasienergy levels, and it is well approximated by Eq. (8). With increasing ϑ, the spectrum smoothly transforms to a set of quasi-Lorenzian peaks corresponding to the linearized approximation determined by Eq. (12).

Lorenzian approximation (8) and consists of many distinct peaks corresponding to transitions between the quasienergy states. With increasing ϑ, it becomes necessary to solve the kinetic equations taking into account all nondiagonal elements of the density matrix. For rather large ϑ, the solution of the master equation leads to the same result as the linear approximation of Eq. (12) corresponding to the vicinity of each classical stable state. The relative height of the peaks is determined by the occupation probabilities of these stable states. The spectrum defined by Eq. (12) consists of two quasi-Lorenzian peaks located at $\pm\omega_{1,2}$, where $\omega_{1,2}$ are the frequencies of the oscillator motion around the stable states 1 and 2. It is important to mention that a peak at zero frequency is always present in the fluorescence spectrum. This peak is connected with transitions between the classical stable states lying in different regions of the system phase portrait.

Another interesting feature is that in both weak-coupling and small-fluctuation regimes the spectra strongly depend on the value of the external driving field, which is demonstrated in Fig. 4. In particular, in the small-fluctuation regime when Eq. (12) is applicable, the spectrum explicitly depends on n. Obtained within the linearized approximation in the vicinity of each stable state, the spectrum defined by Eq. (12) contains two peaks at nonzero frequency. However, the position of these peaks depends on n and therefore differs for the driving fields below threshold ($f < f_0$) and above threshold ($f > f_0$). At the threshold value of the external field f_0, switching between the most probable states 1 and 2 takes place. In the vicinity of the threshold, $f \approx f_0$, the system can be found in

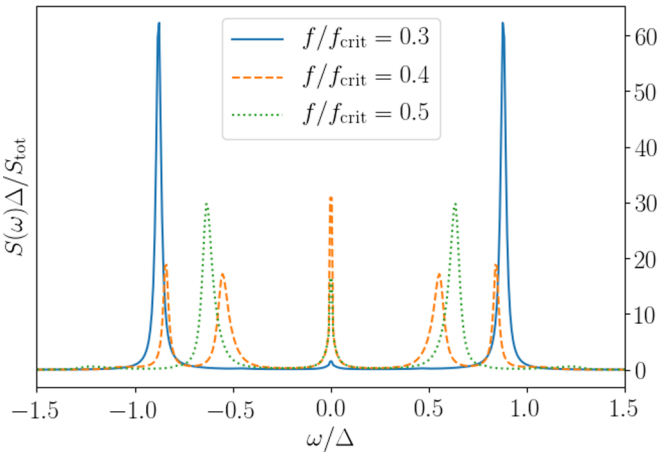

FIG. 4. The fluorescence spectra $S(\omega)$ of the quantum driven nonlinear oscillator are shown for $m = 12.5$, $\vartheta = 0.03$, $N = 0$, and varying values of f. The spectra are normalized by the total fluorescence intensity $S_{\text{tot}} \equiv \int \frac{d\omega}{2\pi} S(\omega)$. For the external fields below threshold ($f/f_{\text{crit}} = 0.3$) and above threshold ($f/f_{\text{crit}} = 0.5$), two symmetric side peaks at nonzero frequencies corresponding to different classical stable states are present. Near the threshold, the spectrum contains four side peaks corresponding to both classical stable states.

both stable states with comparable probabilities, and the total spectrum contains contributions from both of them. Therefore, the spectrum exhibits a crossover when the external field passes the threshold value. Below the threshold, it contains two peaks at frequencies $\pm\omega_1$ corresponding to the stable state 1; in the vicinity of the threshold, it contains four peaks at frequencies $\pm\omega_1$ and $\pm\omega_2$ corresponding to both stable states; and above the threshold, there are two peaks again at frequencies $\pm\omega_2$ corresponding to the stable state 2. Similar arguments can be applied to the weak-coupling regime. The occupation numbers of the eigenstates also differ drastically for $f < f_0$ and $f > f_0$, and different quasienergy states contribute to the spectrum in these cases.

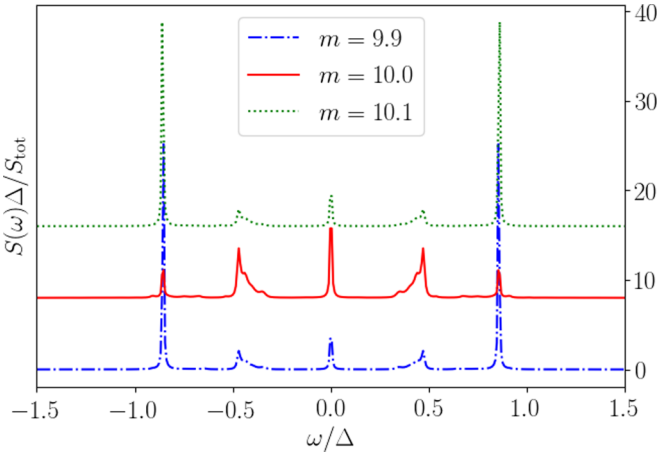

FIG. 5. The fluorescence spectra of the quantum driven nonlinear oscillator are shown for $f/f_{\text{crit}} = 0.29$, $\vartheta = 0.005$, $N = 0$, and varying values of m. For clarity, different spectra are shifted vertically by arbitrary constants. With varying m, the relative heights of the peaks corresponding to different classical stable states strongly change.

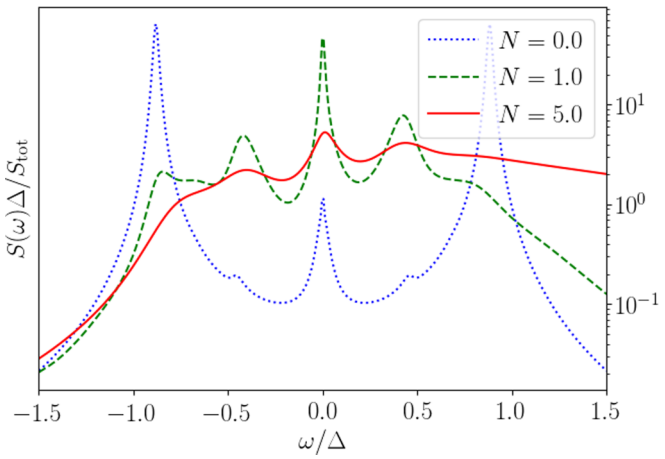

FIG. 6. The fluorescence spectra are depicted for $f/f_{\rm crit} = 0.29$, $\vartheta = 0.03$, $m = 12.5$, and varying N. Mirror symmetry with respect to the vertical axis is present at $N = 0$, and it is violated at $N \neq 0$.

Also, we considered the behavior of spectra near the integer values of the ratio between double detuning and nonlinearity m (see Fig. 5). As shown in Ref. [15], at integer values of m the multiphoton resonance leads to the enhanced probability of the system to occupy the classical stable state with higher amplitude. This could be interpreted as a decrease in the threshold value f_0 of the driving field near the integer values of m. So, varying m changes the relative heights of the peaks corresponding to different classical stable states. When m is close to an integer, the height of the spectrum peaks corresponding to the stable state 2 abruptly increases, whereas the magnitude of the peaks corresponding to the stable state 1 strongly decreases.

In addition, we considered the spectra at different bath temperatures. As can be seen in Fig. 6, the spectra are perfectly symmetric at $N = 0$ and become asymmetric at $N > 0$.

IV. CONCLUSIONS

The fluorescence spectra of a bistable driven system were studied analytically and numerically by means of the Keldysh diagram technique in pseudoparticle representation. The spectra exhibit a smooth transition between the ultraquantum and the quasiclassical limits. It was shown that fluorescence spectra indicate the external field threshold value which corresponds to switching between the most probable states of a bistable system. Moreover, in the vicinity of the external field threshold value the system can be found with comparable probabilities in both stable states. Thus, nearly equal contributions from both states can be clearly seen in the total spectrum. So, it is possible to determine the most probable state of the system from fluorescence spectra in a wide range of external field intensities. In addition, it was revealed that, at integer and half-integer values of the detuning-nonlinearity ratio, multiphoton resonance leads to an enhanced probability of the system to occupy the classical stable state with higher amplitude. So, when this ratio is close to an integer or a half-integer, the height of the spectrum peaks corresponding to the stable state 2 with higher amplitude abruptly increases, whereas the magnitude of the peaks corresponding to the stable state 1 with lower amplitude strongly decreases. Also, we found out that the fluorescence spectra are symmetric at zero bath temperature, and this symmetry breaks down with increasing temperature.

ACKNOWLEDGMENTS

This work was supported by RFBR Grants No. 19-02-000-87a, No. 18-29-20032mk, and No. 19-32-90169 and by a grant 19-1-5-73-1 from the Foundation for the Advancement of Theoretical Physics and Mathematics "BASIS".

APPENDIX A: THE DERIVATION OF THE MASTER EQUATION

The Hamiltonian $\hat{H}_0$ can be diagonalized so that $|n\rangle$ is the set of its eigenvectors. It is convenient to introduce the pseudoparticle operators $\hat{c}_n^\dagger$ and $\hat{c}_n$ which correspond to creation and annihilation of the system eigenstates $|n\rangle$. This implies the constraint on the space of possible physical states: $\sum_n \hat{c}_n^\dagger \hat{c}_n = \mathbb{1}$. The operators $\hat{H}_0$, $\hat{a}$, and $\hat{a}^\dagger$ can be expressed through the pseudoparticle creation and annihilation operators $\hat{c}_n^\dagger$ and $\hat{c}$:

$$\hat{H}_0 = \sum_n \epsilon_n \hat{c}_n^\dagger \hat{c}_n,$$
$$\hat{a} = \sum_{nn'} a_{nn'} \hat{c}_n^\dagger \hat{c}_{n'}. \tag{A1}$$

Although it does not affect physical results, we assume that the pseudoparticles are fermions. We derive the kinetic equation for the density matrix of the system which is directly related to the $G^<(t,t')$ Green's function: $\rho_{nn'}(t) = -iG^<_{nn'}(t,t)$.

The constraint on the Hilbert space, which means the presence of exactly one pseudoparticle in the system, leads to the following additional rules for constructing the Keldysh diagram technique [19,20]:

(i) Among all diagrams only the diagrams with one $G_0^<$ line are kept, which denotes a one-particle Green's function of the noninteracting system.

(ii) If $G^<$ is present in some diagram, the other Green's functions cannot contain the pseudoparticle occupation numbers. Therefore, in all diagrams containing $G^<$, the Green's function $G^>$ reduces to $G^R - G^A$, and the self-energy parts for $G^{R,A}$ also don not contain $G^<$.

In the self-consistent Born approximation, diagrams for G^R, G^A, and $G^<$ are shown in Fig. 7. In the case of white noise, the diagrams with crossing bath Green's functions (shown by dashed lines in Fig. 7) vanish, which provides the validity of the Born approximation. The diagram with crossing lines depicted in Fig. 7 is of the order of $\gamma\tau_c$ compared to noncrossing diagrams, where τ_c is the noise correlation time. This is clear from time representation: for diagrams with crossings, the integration domain is restricted by τ_c. The sum of all diagrams depicted in Fig. 7 can be represented by the following self-consistent equations:

$$G^< = (1 + G^R\Sigma^R)G_0^<(1 + \Sigma^A G^A) + G^R\Sigma^< G^A,$$
$$G^R = G_0^R + G_0^R\Sigma^R G^R, \tag{A2}$$
$$G^A = G_0^A + G^A\Sigma^A G_0^A,$$

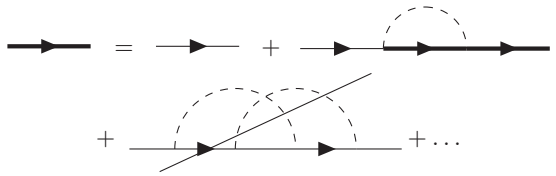

FIG. 7. Graphical representation of the Dyson equation for G^R, G^A, and $G^<$ is shown. The thin solid line corresponds to the pseudoparticle Green's function, the thick solid line corresponds to the dressed pseudoparticle Green's function, the dashed line corresponds to the bath correlation function. Diagrams with crossing bath correlation function lines give contributions proportional to $\gamma\tau_c$ and are neglected in the Dyson equation.

where $(G_0^{R,A})_{nn'}(t,t') = \mp ie^{-i\epsilon_n(t-t')}\theta[\pm(t-t')]\delta_{nn'}$, $(G_0^<)_{nn'}(t,t') = ie^{-i\epsilon_n(t-t')}n_n\delta_{nn'}$, n_n are pseudoparticle occupation numbers, $\Sigma^{R,A}$ are sums of irreducibble diagrams containing no $G_0^<$ lines, and $\Sigma^<$ is the sum of irreducible diagrams containing exactly one $G_0^<$ line. In the self-consistent approximation, they can be expressed as

$$\Sigma_{ij}^{R(A)}(t,t') = i\sum_{kl} a_{ik}G_{kl}^{R(A)}(t,t')D^{>(<)}(t,t')a_{jl}^* + a_{ki}^*G_{kl}^{R(A)}(t,t')D^{<(>)}(t',t)a_{lj}, \tag{A3}$$

$$\Sigma_{ij}^<(t,t') = i\sum_{kl} a_{ik}G_{kl}^<(t,t')D^>(t,t')a_{jl}^* + i\sum_{kl} a_{ki}^*G_{kl}^<(t,t')D^<(t,t')a_{lj}, \tag{A4}$$

where

$$D^<(t,t') = -i\langle\hat\xi^\dagger(t')\hat\xi(t)\rangle, \quad D^>(t,t') = -i\langle\hat\xi(t)\hat\xi^\dagger(t')\rangle, \tag{A5}$$

and the correlation functions of $\hat\xi$ and $\hat\xi^\dagger$ are defined by Eq. (3). By applying $G_0^{-1} \equiv i\partial_t - \hat H_0$ to the first equation of Eqs. (A2) from the left and from the right, one gets the following equation:

$$(i\partial_t + i\partial_{t'} - \epsilon_n + \epsilon_{n'})G_{nn'}^<(t,t') = \int dt''\,[\Sigma^R(t,t'')G^<(t'',t') + \Sigma^<(t,t'')G^A(t'',t') - G^R(t,t'')\Sigma^<(t'',t') - G^<(t,t'')\Sigma^A(t'',t')]_{nn'}, \tag{A6}$$

where the self-energies Σ^R, Σ^A, and $\Sigma^<$ are defined as

$$\Sigma_{n_1n_2}^{R(A)}(t,t') = \frac{i\gamma\delta(t-t')}{2}[(1+N)(\hat a^\dagger\hat a)_{n_1n_2} + N(\hat a\hat a^\dagger)_{n_1n_2}], \tag{A7}$$

$$\Sigma_{n_1n_2}^< = \gamma\delta(t-t')[(1+N)a_{n_1k}G_{kk'}^<(t,t)a_{n_2k'}^* + Na_{kn_1}^*G_{kk'}^<(t,t)a_{k'n_2}]. \tag{A8}$$

In the above equation and below, we omit the summation over repeating indices. After substituting these expressions into Eq. (A6), we obtained exactly the quantum master equation

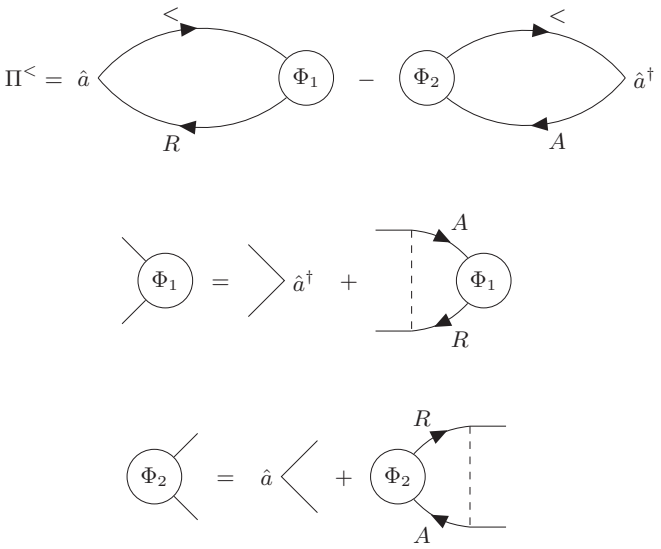

FIG. 8. Diagram ladder representing the polarization operator $\Pi^<$ is shown. Solid lines represent pseudoparticle fermion Green's functions, dashed lines represent bath Green's functions, and circles denote effective vertices $\Phi_{1,2}$.

for the δ-correlated bath:

$$(i\partial_t - \epsilon_i + \epsilon_j)G_{nn'}^<(t,t) = \frac{i\gamma(1+N)}{2}[2a_{nk}a_{n'l}^* - (\hat a^\dagger\hat a)_{nk}\delta_{n'l} - \delta_{nk}(\hat a^\dagger\hat a)_{n'l}]G_{kl}^<(t,t) + \frac{i\gamma N}{2}[2a_{kn}^*a_{ln'} - (\hat a\hat a^\dagger)_{nk}\delta_{n'l} - \delta_{nk}(\hat a\hat a^\dagger)_{n'l}]G_{kl}^<(t,t). \tag{A9}$$

Equation (A9) is equivalent to the quantum master equation, Eq. (4):

$$\partial_t\rho_{nn'} = (\mathcal{L}\rho)_{nn'} = -i(\epsilon_n - \epsilon_{n'})\rho_{nn'} + \frac{\gamma}{2}(2a\rho a^\dagger - \rho a^\dagger a - a^\dagger a\rho + 2N[[a,\rho],a^\dagger])_{nn'}. \tag{A10}$$

APPENDIX B: POLARIZATION OPERATOR

The polarization operator $\Pi^<(t,t') \equiv \langle \mathrm{T}_C\hat a_-(t)\hat a_+^\dagger(t')\rangle$ is represented as a sum of diagrams shown in Fig. 8. For white external noise, it consists of a ladder of diagrams without crossing bath propagators. The sum of all such diagrams can be calculated in a way similar to that of the Bethe-Salpether equation.

In steady state, $\Pi^<(t,t')$ depends only on $t-t'$. Thus, in ω representation the graphical equations shown in Fig. 8 take the following form:

$$\Pi^<(\omega) = \int\frac{d\omega'}{2\pi}\,\mathrm{Tr}\,\hat aG^<(\omega+\omega')\Phi_1(\omega)G^R(\omega') - \int\frac{d\omega'}{2\pi}\,\mathrm{Tr}\,\Phi_2(\omega)G^<(\omega'+\omega)\hat a^\dagger G^A(\omega'), \tag{B1}$$

where $G^R(\omega)$ and $G^A(\omega)$ are the solutions of Eqs. (A2) in Fourier representation. The stationary Green's

function $G^<(\omega)$ obtained from these equations takes the form $G^<(\omega)_{ij} = [\rho_{\rm st} G^A(\omega)]_{ij} - [G^R(\omega)\rho_{\rm st}]_{ij}$, $(\rho_{\rm st})_{ij} \equiv -i\int \frac{d\omega}{2\pi} G^<(\omega)_{ij}$. The vertex functions $\Phi_1(\omega)$ and $\Phi_2(\omega)$ read as follows:

$$\Phi_1(\omega)_{kl} = a^*_{lk} + \gamma \int \frac{d\omega'}{2\pi}(1+N) \times [\hat{a} G^A(\omega+\omega')\Phi_1(\omega) G^R(\omega')\hat{a}^\dagger]_{kl} + N[\hat{a}^\dagger G^A(\omega+\omega')\Phi_1(\omega) G^R(\omega')\hat{a}]_{kl}, \quad \text{(B2)}$$

$$\Phi_2(\omega)_{kl} = a_{kl} + \gamma \int \frac{d\omega'}{2\pi}(1+N) \times [\hat{a} G^A(\omega')\Phi_2(\omega) G^R(\omega'+\omega)\hat{a}^\dagger]_{kl} + N[\hat{a}^\dagger G^A(\omega')\Phi_2(\omega) G^R(\omega'+\omega)\hat{a}]_{kl}. \quad \text{(B3)}$$

From Eqs. (B2) and (B3), one could obtain $\Phi_{1,2}(\omega)$ explicitly. For this, it is convenient to introduce tensor notation for denoting superoperators acting on operators, because the space of operators acting on a Hilbert space is isomorphic to the tensor product of a Hilbert space and its conjugate. For example, the combination $\hat{a}G^A(\omega')\Phi_2(\omega)G^R(\omega+\omega')\hat{a}^\dagger$ can be written using this notation as $\{\hat{a}G^A(\omega') \otimes [G^R(\omega+\omega')\hat{a}^\dagger]^T\}\Phi_2(\omega)$: This means that the operator $\hat{a}G^A(\omega') \otimes [G^R(\omega+\omega')\hat{a}^\dagger]^T$ acting on the tensor product of a Hilbert space and its conjugate is multiplied on Φ_2 which is considered as a vector from the tensor product.

Using this notation, one gets the following expressions for $\Phi_{1,2}$:

$$\Phi_1(\omega) = \left\{\mathbb{1}\otimes\mathbb{1} - \gamma\int \frac{d\omega'}{2\pi}[(1+N)\hat{a}^\dagger \otimes \hat{a}^T + N\hat{a}\otimes(\hat{a}^\dagger)^T] G^A(\omega+\omega') \otimes G^R(\omega')^T\right\}^{-1} \hat{a}^\dagger, \quad \text{(B4)}$$

$$\Phi_2(\omega) = \left\{\mathbb{1}\otimes\mathbb{1} - \gamma\int \frac{d\omega'}{2\pi}[(1+N)\hat{a}^\dagger \otimes \hat{a}^T + N\hat{a}\otimes(\hat{a}^\dagger)^T] G^A(\omega') \otimes G^R(\omega+\omega')^T\right\}^{-1} \hat{a}. \quad \text{(B5)}$$

Using Eqs. (B1), (B4), and (B5), it is possible to calculate the polarization operator in a closed form. Moreover, all these equations contain the integral of the product of retarded and advanced Green's functions. For this integral, the following identity holds:

$$\int \frac{d\omega'}{2\pi} G^A(\omega') \otimes G^R(\omega'+\omega) = \left\{-i\omega - i\hat{H}\otimes\mathbb{1} + i\mathbb{1}\otimes\hat{H} + \frac{\gamma}{2}[(1+N)a^\dagger a + Na^\dagger a]\otimes\mathbb{1} + \frac{\gamma}{2}\mathbb{1}\otimes[(1+N)a^\dagger a + Na^\dagger a]\right\}^{-1}. \quad \text{(B6)}$$

The above equation can be proven in time representation by differentiating the product $G^A(-t)\otimes G^R(t)$ by t. To get the final expression for $\Pi^<$, one should substitute Eq. (B6) into Eqs. (B4) and (B5), and then substitute Eqs. (B4) and (B5) into Eq. (B1). Thus, the polarization operator $\Pi^<$ reads

$$\Pi^< = {\rm Tr}[\hat{a}^\dagger\{-i\omega\mathbb{1} - \mathcal{L}\}(\hat{a}\hat{\rho}_{\rm st})] + {\rm Tr}[\hat{a}\{i\omega\mathbb{1} - \mathcal{L}\}(\hat{\rho}_{\rm st}\hat{a}^\dagger)], \quad \text{(B7)}$$

where

$$\mathcal{L} = -i\hat{H}_0\otimes\mathbb{1} + i\mathbb{1}\otimes\hat{H}_0^T + \frac{\gamma(1+N)}{2}[2\hat{a}\otimes(\hat{a}^\dagger)^T - \hat{a}^\dagger\hat{a}\otimes\mathbb{1} - \mathbb{1}\otimes(\hat{a}^\dagger\hat{a})^T] + \frac{\gamma N}{2}[2\hat{a}^\dagger\otimes\hat{a}^T - \hat{a}\hat{a}^\dagger\otimes\mathbb{1} - \mathbb{1}\otimes(\hat{a}\hat{a}^\dagger)^T]. \quad \text{(B8)}$$

The calculations above can be considerably simplified in the limit of small γ. In this limit, the density matrix of the system can be calculated in the diagonal approximation as well as G^R and G^A:

$$\rho_{nn'} = P_n\delta_{nn'}, \quad G^{R,A}_{nn'} = (\omega - \epsilon_n \pm \gamma_n)^{-1}\delta_{nn'}, \quad \gamma_n = \frac{\gamma}{2}[(1+N)\hat{a}^\dagger\hat{a} + N\hat{a}\hat{a}^\dagger]_{nn}. \quad \text{(B9)}$$

When ω is close to the difference between some energy levels $E_n - E_{n'}$, the diagonal approximation for $G^{R,A}$ can be used for calculating Φ_1, Φ_2, and $\Pi^<$. Retaining only diagonal retarded and advanced Green's functions in Eqs. (B6), one can obtain

$$\int \frac{d\omega'}{2\pi} G^A_{n'n'}(\omega')G^R_{nn}(\omega'+\omega) = \frac{i}{\omega - \epsilon_n + \epsilon_{n'} + i(\gamma_n+\gamma_{n'})}. \quad \text{(B10)}$$

This allows one to calculate $\Phi_{1,2}$ in resonant approximation from Eqs. (B2) and (B3):

$$(\Phi_1)_{kl} = a^*_{lk}\left(1 + \frac{i\Delta\gamma_{kl}}{\omega - \epsilon_k + \epsilon_l - i(\gamma_k+\gamma_l)}\right)^{-1}, \quad (\Phi_2)_{kl} = a_{kl}\left(1 - \frac{i\Delta\gamma_{kl}}{\omega - \epsilon_k + \epsilon_l + i(\gamma_k+\gamma_l)}\right)^{-1}, \quad \Delta\gamma_{kl} = \gamma[(1+N)a_{kk}a^*_{ll} + Na^*_{kk}a_{ll}]. \quad \text{(B11)}$$

Keeping also only G^R_{nn} and $G^A_{n'n'}$ in $\Pi^<$ given by Eq. (B1), one derives Eq. (8) where $\Gamma_{nn'} = \gamma_n + \gamma_{n'} - \Delta\gamma_{nn'}$ [see Eq. (9)].

Thus, the spectrum in the limit of small γ consists of multiple narrow Lorentz peaks corresponding to transitions between the system eigenstates. From Eq. (9), the linewidth narrowing for the transitions between two well-defined quasienergy states can be seen. It appears from summing the

series of ladder diagrams in the polarization operator $\Pi^<$, and the linewidth differs from the sum of the widths γ_n and $\gamma_{n'}$ of the quasienergy states involved in the transition (see Fig. 2). In addition, the Keldysh diagram technique allows one to treat the corrections arising from finite bath correlation time τ_c in a regular way. In the Keldysh diagram technique approach, such corrections are represented by subseries of maximally crossing diagrams similar to cooperons in the theory of weak localization and are proportional to correlation time in the leading order. These diagrams are of order $\gamma\tau_c$ compared to noncrossing ladder diagrams contributing to the leading-order approximation.

[1] R. Bonifacio and L. A. Lugiato, Phys. Rev. A **18**, 1129 (1978).
[2] N. A. Gippius, I. A. Shelykh, D. D. Solnyshkov, S. S. Gavrilov, Y. G. Rubo, A. V. Kavokin, S. G. Tikhodeev, and G. Malpuech, Phys. Rev. Lett. **98**, 236401 (2007).
[3] H. M. Gibbs, S. L. McCall, and T. N. C. Venkatesan, Phys. Rev. Lett. **36**, 1135 (1976).
[4] S. L. McCall, Phys. Rev. A **9**, 1515 (1974).
[5] V. Braginsky, M. Gorodetsky, and V. Ilchenko, Phys. Lett. A **137**, 393 (1989).
[6] T. Boulier, M. Bamba, A. Amo, C. Adrados, A. Lemaitre, E. Galopin, I. Sagnes, J. Bloch, C. Ciuti, E. Giacobino, and A. Bramati, Nat. Commun. **5**, 3260 (2014).
[7] P. R. Muppalla, O. Gargiulo, S. I. Mirzaei, B. P. Venkatesh, M. L. Juan, L. Grunhaupt, I. M. Pop, and G. Kirchmair, Phys. Rev. B **97**, 024518 (2018).
[8] H. Risken, C. Savage, F. Haake, and D. F. Walls, Phys. Rev. A **35**, 1729 (1987).
[9] K. Vogel and H. Risken, Phys. Rev. A **42**, 627 (1990).
[10] N. S. Maslova, E. V. Anikin, N. A. Gippius, and I. M. Sokolov, Phys. Rev. A **99**, 043802 (2019).
[11] N. S. Maslova, E. V. Anikin, V. N. Mantsevich, N. A. Gippius, and I. M. Sokolov, Laser Phys. Lett. **16**, 045205 (2019).
[12] P. D. Drummond and D. F. Walls, J. Phys. A: Math. Gen. **13**, 725 (1980).
[13] L. M. Narducci, R. Gilmore, D. H. Feng, and G. S. Agarwal, Opt. Lett. **2**, 88 (1978).
[14] T. Weißl, B. Küng, E. Dumur, A. K. Feofanov, I. Matei, C. Naud, O. Buisson, F. W. J. Hekking, and W. Guichard, Phys. Rev. B **92**, 104508 (2015).
[15] E. V. Anikin, N. S. Maslova, N. A. Gippius, and I. M. Sokolov, Phys. Rev. A **100**, 043842 (2019).
[16] H. Haken, Z. Phys. **219**, 411 (1965).
[17] H. Risken, Z. Phys. **186**, 85 (1965).
[18] H. Haken, Z. Phys. **219**, 246 (1969).
[19] P. Arseyev and N. S. Maslova, JETP Lett. **100**, 197 (2014).
[20] P. I. Arseev, Usp. Fiz. Nauk **185**, 1271 (2015).